HHS Public Access

Author manuscript

Nat Genet. Author manuscript; available in PMC 2016 September 22.

Published in final edited form as:

Nat Genet. 2016 June ; 48(6): 675–680. doi:10.1038/ng.3549.

Recurrent activating mutations of G-protein-coupled receptor *CYSLTR2* in uveal melanoma

Amanda R Moore[1,2], **Emilie Ceraudo**[3], **Jessica J Sher**[1], **Youxin Guan**[1], **Alexander N Shoushtari**[4,5], **Matthew T Chang**[1,6,7], **Jenny Q Zhang**[1], **Edward G Walczak**[1], **Manija A Kazmi**[3], **Barry S Taylor**[1,6,8], **Thomas Huber**[3], **Ping Chi**[1,2,4,5], **Thomas P Sakmar**[3,9], and **Yu Chen**[1,2,4,5]

[1]Human Oncology and Pathogenesis Program, Memorial Sloan Kettering Cancer Center, New York, New York, USA

[2]Weill Cornell Graduate School of Medical Sciences, Cornell University, New York, New York, USA

[3]Laboratory of Chemical Biology and Signal Transduction, Rockefeller University, New York, New York, USA

[4]Department of Medicine, Memorial Sloan Kettering Cancer Center, New York, New York, USA

[5]Department of Medicine, Weill Cornell Medical College, New York, New York, USA

[6]Department of Epidemiology and Biostatistics, Memorial Sloan Kettering Cancer Center, New York, New York, USA

[7]Department of Bioengineering and Therapeutic Sciences, University of California, San Francisco, San Francisco, California, USA

[8]Marie-Josée and Henry R. Kravis Center for Molecular Oncology, Memorial Sloan Kettering Cancer Center, New York, New York, USA

[9]Department of Neurobiology, Care Sciences and Society, Division for Neurogeriatrics, Center for Alzheimer Research, Karolinska Institutet, Huddinge, Sweden

Abstract

Uveal melanomas are molecularly distinct from cutaneous melanomas and lack mutations in *BRAF*, *NRAS*, *KIT*, and *NF1*. Instead, they are characterized by activating mutations in *GNAQ* and *GNA11*, two highly homologous α subunits of $G_{\alpha q/11}$ heterotrimeric G proteins, and in

Correspondence should be addressed to Y.C. (cheny1@mskcc.org).

AUTHOR CONTRIBUTIONS

Project planning and experimental design: P.C., Y.C., A.R.M., T.P.S., M.A.K., and E.C. Bioinformatic analysis of exome sequencing data: Y.C., A.R.M., M.T.C., and B.S.T. Clinical specimen acquisition, annotation, and analysis: A.N.S. Immunoblots, growth curves, qPCR, and all cellular assays: A.R.M., E.C., and Y.G. Xenograft assays: A.R.M., J.J.S., and E.G.W. Generation of the expression vectors: J.Q.Z., E.C., and A.R.M. Molecular modeling: T.H. Manuscript writing: A.R.M., P.C., Y.C., E.C., and T.P.S. All authors reviewed the final manuscript.

COMPETING FINANCIAL INTERESTS

The authors declare no competing financial interests.

PLCB4 (phospholipase C β4), the downstream effector of $G_{\alpha q}$ signaling [1–3]. We analyzed genomics data from 136 uveal melanoma samples and found a recurrent mutation in *CYSLTR2* (cysteinyl leukotriene receptor 2) encoding a p.Leu129Gln substitution in 4 of 9 samples that lacked mutations in *GNAQ*, *GNA11*, and *PLCB4* but in 0 of 127 samples that harbored mutations in these genes. The Leu129Gln $CysLT_2R$ mutant protein constitutively activates endogenous $G_{\alpha q}$ and is unresponsive to stimulation by leukotriene. Expression of Leu129Gln $CysLT_2R$ in melanocytes enforces expression of a melanocyte-lineage signature, drives phorbol ester–independent growth *in vitro*, and promotes tumorigenesis *in vivo*. Our findings implicate *CYSLTR2* as a uveal melanoma oncogene and highlight the critical role of $G_{\alpha q}$ signaling in uveal melanoma pathogenesis.

Uveal melanomas arise from melanocytes of the uveal tract and are the most prevalent tumors of the eye. To identify additional oncogenic drivers in uveal melanoma, we curated whole-genome or whole-exome sequencing data for 136 uveal melanomas from The Cancer Genome Atlas (TCGA, personal communication), Cancer Research UK (CRUK) [4], QIMR Berghofer Medical Research Institute (QIMR) [3], and University of Duisburg-Essen (UNI-UDE) [5] cohorts. We performed mutational analysis using an algorithm that is highly sensitive in detecting rare hotspot mutations found in oncogenes [6]. We identified seven significantly mutated ($q < 0.05$) codons in six genes, including known mutations in *GNAQ*, *GNA11*, *PLCB4*, *SF3B1*, and *EIF1AX*. In addition, we found a new c.386T>A mutation in *CYSLTR2* encoding a p.Leu129Gln substitution in four samples ($q = 3.3 \times 10^{-8}$) (Fig. 1a, Table 1, and **Supplementary Fig. 1a**). RNA-seq data validated the presence of the *CYSLTR2* mutation encoding p.Leu129Gln and confirmed expression of the mutant allele (**Supplementary Figs. 1a and 2c**). For further validation, we performed Sanger sequencing on two Memorial Sloan Kettering Cancer Center (MSKCC) patient samples that lacked *GNAQ* and *GNA11* mutations (2/28) and found one sample with a *CYSLTR2* mutation encoding p.Leu129Gln (**Supplementary Fig. 1b**). Although *CYSLTR2* is sporadically mutated in other cancer types sequenced by TCGA, these mutations do not occur at hotspots (except for mutations mapping to Arg136 (p.Arg136Cys or p.Arg136His) in three samples), the corresponding transcripts are not expressed at high levels, and the mutations are found in high-mutation-burden tumors, suggesting that *CYSLTR2* might not be an oncogenic driver in other tumor types and that the *CYSLTR2* hotspot mutation encoding p.Leu129Gln is unique to uveal melanoma (**Supplementary Fig. 2**).

Because mutations that activate the same pathway or mutations that define molecular subtypes tend to be mutually exclusive, we used CoMEt to identify mutually exclusive mutational modules *de novo* in the data set with 136 uveal melanomas [7]. We found that mutations in *GNAQ*, *GNA11*, *PLCB4*, and *CYSLTR2* formed a highly significantly mutually exclusive module ($P = 4.2 \times 10^{-33}$), suggesting that these genes are in the same pathway. *BAP1* (ref. 8), *SF3B1*, and *EIF1AX* formed a second mutually exclusive module ($P = 2.0 \times 10^{-5}$), consistent with the observation that *BAP1* mutations primarily occur in tumors with monosomy 3 and *SF3B1* and *EIF1AX* mutations primarily occur in tumors with disomy 3 (Fig. 1b) [5, 9].

CYSLTR2 encodes cysteinyl leukotriene receptor 2 ($CysLT_2R$), a seven-transmembrane G-protein-coupled receptor (GPCR), which functions in leukotriene-mediated signaling, including during inflammation and fibrosis. $CysLT_2R$ belongs to the rhodopsin-like family of GPCRs and is known to activate $G_{\alpha q}$ (Fig. 1c) [10, 11]. Leu129 of $CysLT_2R$ is located in transmembrane helix 3 (TM3), a functional hub of the receptor that makes contact with the ligand extracellularly, associates with other transmembrane helices within the membrane, and interacts with the G_{α} subunit intracellularly (Fig. 2a). Leu129 resides in the highly conserved 3.43 position (Ballesteros–Weinstein numbering [12]) that stabilizes the inactive configuration of GPCRs through intramolecular contacts. Alteration at the 3.43 position has been shown to confer constitutive activity in a number of GPCRs, including the β-adrenergic, luteinizing hormone, and thyroid-stimulating hormone receptors [13]. To further understand the role of Leu129, we modeled the structure of $CysLT_2R$ on the basis of the known structure of its close homolog, protease-activated receptor 1 (PAR1) [14]. Leu129 (3.43) resides in a hydrophobic core of the GPCR, which is highly enriched in hydrophobic residues (Leu80 (1.45), Ser125 (3.39), Leu132 (3.46), Thr252 (6.41), Ile255 (6.44), Phe256 (6.45), Phe260 (6.49), Asn297 (7.45), Asn301 (7.49), and Leu304 (7.52)) (Fig. 2a), suggesting that substitution with a more hydrophilic glutamine residue (p.Leu129Gln) might disrupt structural organization.

To determine the ability of the wild-type and Leu129Gln $CysLT_2R$ proteins to couple with $G_{\alpha q}$, we generated synthetic genes encoding wild-type *CYSLTR2* and the mutant, transiently expressed them in HEK293 T cells, and measured calcium mobilization (Fig. 2b). Leukotriene D_4 (LTD_4), a potent $CysLT_2R$ agonist, mobilized calcium in cells expressing wild-type $CysLT_2R$ but not in those transfected with empty vector, in a concentration-dependent manner. Cells expressing Leu129Gln $CysLT_2R$ exhibited high basal calcium levels that were not augmented by increasing concentrations of LTD_4, indicating that the receptor is constitutively active (Fig. 2b,c). Wild-type and Leu129Gln $CysLT_2R$ were expressed at similar levels, as determined by immunoblot analysis for the engineered N-terminal FLAG and C-terminal 1D4 tags, and the proteins demonstrated similar cellular localization by immunofluorescence and similar levels of cell surface expression by FACS analysis (for extracellular FLAG epitope), suggesting that the different functional behavior of the mutant is not due to different expression level or localization in comparison with the wild-type receptor (**Supplementary Fig. 3a–c**). To determine whether wild-type and Leu129Gln $CysLT_2R$ are coupled to the $G_{\alpha s}$ activating or $G_{\alpha i}$ inhibitory adenylyl cyclase pathway, we measured the ligand-mediated increase in cAMP levels, indicative of $G_{\alpha s}$ coupling, and the ligand-mediated decrease in forskolin-induced cAMP levels, indicative of $G_{\alpha i}$ coupling. The basal level of cAMP was not altered by expression of either wild-type or Leu129Gln $CysLT_2R$; further, addition of LTD_4 did not increase cAMP levels in cells expressing wild-type or Leu129Gln $CysLT_2R$ (Fig. 2d), arguing against coupling of Leu129Gln $CysLT_2R$ with $G_{\alpha s}$. After stimulation with forskolin, LTD_4 minimally inhibited the increase in cAMP levels in cells expressing wild-type $CysLT_2R$ in comparison to those transfected with vector control, but cAMP levels were unaffected by LTD_4 in cells expressing Leu129Gln $CysLT_2R$ (Fig. 2e), indicating that Leu129Gln $CysLT_2R$ was not coupled with $G_{\alpha i}$. These data, in combination with the calcium flux data, suggest that Leu129Gln $CysLT_2R$ is a gain-of-function mutant that primarily couples through $G_{\alpha q}$.

To determine whether Leu129Gln $CysLT_2R$ possesses oncogenic properties, we stably expressed empty-vector control, wild-type $CysLT_2R$, and Leu129Gln $CysLT_2R$, as well as the Arg136His $CysLT_2R$ mutant receptor found in three independent TCGA samples (**Supplementary Fig. 2b**), in immortalized mouse NIH3T3 fibroblasts and subcutaneously grafted these cells into severe combined immunodeficient (SCID) mice. We found that only cells expressing Leu129Gln $CysLT_2R$ were able to form tumors *in vivo* (**Supplementary Fig. 4a**), indicating that Leu129Gln $CysLT_2R$ has oncogenic activities.

To determine the melanocyte-lineage-specific effects of the $CysLT_2R$ p.Leu129Gln substitution, we stably expressed the empty-vector control, wild-type $CysLT_2R$, and Leu129Gln $CysLT_2R$ in melan-a cells, an immortalized mouse melanocytic cell line. Melan-a cells require phorbol esters such as 12-*O*-tetradecanoylphorbol-13-acetate (TPA) for growth [15]. Leu129Gln but not wild-type $CysLT_2R$ conferred TPA-independent growth (Fig. 3a).

We next sought to phenotypically characterize expression of Leu129Gln $CysLT_2R$ in the melanocyte lineage. In addition to being required for growth, supplemental TPA promotes melanocyte-lineage specification and pigmentation in both human and mouse melanocytes [16, 17]. Notably, Leu129Gln $CysLT_2R$ expression dramatically augmented pigmentation in melan-a cells cultured in TPA-containing medium, with increased numbers of large pigmented melanosomes (Fig. 3b). When TPA was withdrawn, melan-a cells lost cytoplasmic branches and became rounded within 72 h and pigmentation was completely lost over 18 d (Fig. 3b,c and **Supplementary Fig. 4b**). Remarkably, Leu129Gln $CysLT_2R$ expression rescued both pigmentation and cell morphology (Fig. 3b,c). We next assayed for expression of melanocyte-lineage-specific genes (for example, *Mitf*, *Kit*, and *Dct*) and found that their expression was decreased upon TPA withdrawal. Leu129Gln $CysLT_2R$ expression modestly increased expression of these genes in the presence of TPA but dramatically increased their expression in the absence of TPA (Fig. 3d,e and **Supplementary Fig. 5**). To determine whether Leu129Gln $CysLT_2R$ also promotes melanocyte-lineage specification in the human context, we stably expressed the empty-vector control, wild-type $CysLT_2R$, and Leu129Gln $CysLT_2R$ in MEL290 cells, a human uveal melanoma cell line that is wild type for *GNA11* and *GNAQ* [18]. Expression of Leu129Gln $CysLT_2R$ but not controls significantly increased expression of melanocyte-lineage-specific genes (for example, *DCT*, *TYRP1*, and *TYR*) (Fig. 3f).

To determine the role of the $CysLT_2R$ p.Leu129Gln substitution in melanoma tumorigenesis *in vivo*, we grafted melan-a cells expressing empty-vector control, wild-type $CysLT_2R$, and Leu129Gln $CysLT_2R$ into SCID mice and found that Leu129Gln $CysLT_2R$ significantly accelerated tumor formation in comparison to empty vector ($P < 0.001$; Fig. 4a). Examination of melan-a tumor grafts showed that tumors expressing Leu129Gln $CysLT_2R$ were highly pigmented and expressed higher levels of melanocyte-lineage-specific markers (for example, *Mitf*, *Kit*, *Dct*, *Tyrp1*, and *Tyr*) than grafts expressing empty-vector control and wild-type $CysLT_2R$ (Fig. 4b–e and **Supplementary Fig. 5**). These data indicate that, within the melanocyte lineage, Leu129Gln $CysLT_2R$ enforces a master melanocyte-lineage-specific transcriptional program and promotes transformation.

Because Leu129Gln $CysLT_2R$ conferred TPA-independent growth in melan-a cells, we asked whether melan-a cells expressing Leu129Gln $CysLT_2R$ had become dependent on it for proliferation. We performed small interfering RNA (siRNA)-mediated knockdown of the exogenous human *CYSLTR2* in cells expressing wild-type $CysLT_2R$ and Leu129Gln $CysLT_2R$. Knockdown of *CYSLTR2* reduced growth in cells with Leu129Gln $CysLT_2R$ grown in the presence or absence of TPA and caused the cells to have a flattened morphology, but it did not affect the growth or morphology of cells with wild-type $CysLT_2R$ grown in the presence of TPA (Fig. 5a,b). Further, knockdown of *CYSLTR2* in cells expressing Leu129Gln $CysLT_2R$ decreased the expression of melanocyte-lineage genes (Fig. 5c). These data suggest that inhibiting $CysLT_2R$ in cell lines with the *CYSLTR2* mutation encoding p.Leu129Gln can have therapeutic potential.

GPCR mutations drive several benign endocrine neoplasms, including mutations of thyroid-stimulating hormone receptor in thyroid adenoma [19] and luteinizing hormone receptor in testicular Leydig adenoma [20]. In addition, many GPCRs can be oncogenic in experimental systems, and analysis of whole-exome studies has shown that GPCRs are among the most commonly mutated genes, mutated in approximately 20% of all cancers [21, 22]. Despite the high mutation rate, to our knowledge, no single GPCR has been identified as a significantly mutated gene in any malignant tumor type [23, 24], possibly because GPCR genes generally lack hotspot mutations and mutations in these genes co-occur with mutations in other well-known driver oncogenes. We have defined a recurrent hotspot mutation of *CYSLTR2* in uveal melanoma, which represents a bona fide mutated GPCR driver oncogene. Leu129Gln $CysLT_2R$ exhibits high basal activity and couples through $G_{\alpha q}$, thereby activating a signaling pathway convergent with the one activated by *GNAQ* and *GNA11* oncogenic mutations (Fig. 1c). We further demonstrated that Leu129Gln $CysLT_2R$ enforces expression of the melanocyte-lineage-specific transcriptional program, possibly having a role similar to that of *MITF* amplification in enforcing lineage in cutaneous melanoma [25].

GPCRs are attractive drug targets because of their location on the plasma membrane and the availability of high-throughput cell-based screens for drug discovery. Inhibitors of $CysLT_1R$, such as montelukast, are broadly used in asthma [26]. Unfortunately, montelukast has no activity against $CysLT_2R$. Recently, several compounds have been discovered with purported activity against wild-type $CysLT_2R$, including one that is undergoing phase II clinical trial [27]. Transition of wild-type GPCR between the inactive and active conformations depends on the ligand environment, but mutations conferring constitutive activity strongly bias the protein toward the active conformation, either through destabilization of the inactive state or stabilization of the active state. To inhibit these mutants, high-affinity ‘inverse agonists’ that stabilize the inactive state will be required [28]. Development of such drugs to inhibit Leu129Gln $CysLT_2R$ will have therapeutic potential in uveal melanoma with *CYSLTR2* mutation encoding p.Leu129Gln, a disease that currently has no effective therapy.

URLs. 4Peaks, http://nucleobytes.com/4peaks; NIHTCGA server, https://tcga-data.nci.nih.gov/; hotspots algorithm, https://github.com/taylor-lab/hotspots; CoMEt algorithm, https://github.com/raphael-group/comet/releases; Cancer Genomics Hub, https://cghub.ucsc.edu/; Integrative Genomics Viewer, https://www.broadinstitute.org/igv/; MSKCC

cBioPortal, http://www.cbioportal.org/; SAMtools, http://www.htslib.org/; Bowtie 2, http://bowtie-bio.sourceforge.net/bowtie2/.

ONLINE METHODS

Mutational analysis

Level 2 whole-exome mutational data (curated Broad Institute calls) and Level 3 RNA-seqV2 data from TCGA uveal melanomas ($n = 80$) were downloaded from the NIH TCGA server. Processed whole-exome sequencing data from the UNI-UDE uveal melanoma cohort ($n = 22$) and processed whole-genome sequencing data from the CRUK ($n = 12$) and QIMR ($n = 28$) cohorts were extracted from the supplementary tables of relevant publications [3–5]. For downstream analysis, we merged the data for 3 duplicate samples present in both the CRUK and TCGA databases and removed 3 samples from the QIMR database that lacked any somatic mutations, leaving 136 samples. To identify significant hotspot mutations, we ran an algorithm that is highly sensitive in detecting rare hotspot mutations [6]. To identify and visualize mutually exclusive mutations, we ran the CoMEt algorithm [7] using 10 million iterations and 100 permutations. Statistical significance is represented by mid *P* value (described as Φ in ref. 7). To examine raw DNA and RNA sequencing reads with *CYSLTR2* mutation, we obtained TCGA BAM files from the Cancer Genomics Hub and UNI-UDE fastq files from the European Nucleotide Archive (study accession ERP003230) and mapped reads to the hg19 reference genome using Bowtie 2 (ref. 29). To determine the number of wild-type and mutant reads at *CYSLTR2*, we used SAMtools mpileup after filtering for base quality of at least 13 (ref. 30). Reads were visualized using the Integrative Genomics Viewer [31]. The OncoPrint was generated using MSKCC cBioPortal [32].

For the MSKCC uveal melanoma cohort, all patients provided informed consent for tissue procurement and mutational testing, and the study was approved by the institutional review board (12-245A). Tumor samples were sequenced using MSK-IMPACT, a hybrid-capture deep sequencing assay of 341 key cancer-related genes. The MSK-IMPACT panel includes *GNAQ* and *GNA11* but does not include *CYSLTR2* (ref. 33). We obtained tumor and germline DNA from the MSK-IMPACT sequencing libraries of two patients who lacked mutations in *GNAQ* and *GNA11* and performed Sanger sequencing of *CYSLTR2*.

For pan-TCGA analysis of *CYSLTR2* mutations, we obtained curated data from MSKCC cBioPortal. We examined 24 disease cohorts (**Supplementary Fig. 2a**) and selected cases with both mutational data and RNA-seq-based gene expression data.

Sanger sequencing of *CYSLTR2*

Sequence analysis of codon 129 of *CYSLTR2* by Sanger sequencing was performed by standard PCR using HotStarTaq Plus Master Mix (Qiagen) with *CYSLTR2* Sanger sequencing primers (**Supplementary Table 1**). PCR products were purified using the E.Z.N.A. Cycle Pure kit (Omega) and sent for sequencing with the same primers used for PCR. Sequencing plots were created with 4Peaks.

Exogenous gene expression

For transient expression in HEK293T cells used in *in vitro* assays of calcium mobilization and cAMP accumulation, we generated vectors with synthetic *CYSLTR2* encoding the protein fused to an N-terminal FLAG epitope (DYKDDDDK) and a C-terminal 1D4 epitope (TETSQVAPA) and subcloned this sequence into pcDNA3.1(+) (Life Technologies) using the restriction enzymes EcoRV and NotI (constructed by Genewiz). The human *CYSLTR2* sequence was codon optimized for expression in mammalian cells by Genewiz. The construct encoding Leu129Gln CysLT2R mutant receptor was generated by QuikChange (Agilent Technologies) site-directed mutagenesis of *CYSLTR2* to introduce a c.386T>A mutation (NM_020377.2) encoding the p.Leu129Gln substitution using synthetic *CYSLTR2* L129Q QuikChange primers (**Supplementary Table 1**). HEK293T cells were transfected with the plasmids subcloned into pcDNA3.1(+) using Lipofectamine 2000 (Life Technologies) according to the manufacturer's recommendations. For stable expression in NIH3T3 and melan-a cells, the cDNA for wild-type human *CYSLTR2* was obtained from Origene and cloned into the MSCV-IRES-GFP vector [34] (pMIGw; Addgene plasmid 12282). QuikChange site-directed mutagenesis was performed using *CYSLTR2* L129Q QuikChange primers (**Supplementary Table 1**) on wild-type *CYSLTR2* to introduce a c.386T>A mutation encoding the p.Leu129Gln substitution. In addition, site-directed mutagenesis was performed using *CYSLTR2* R136H QuikChange primers (**Supplementary Table 1**) on wild-type *CYSLTR2* to introduce a c.407G>A mutation encoding the p.Arg136His substitution. The sequences of all constructs were confirmed by sequencing.

Intracellular calcium flux mobilization assays ($G_{\alpha q}$ assays)

HEK293T cells were seeded at a density of 20,000 cells/well in 384-well plates (Corning) coated with poly-d-lysine hydrobromide (Sigma-Aldrich) and transiently transfected with vector encoding wild-type or Leu129Gln CysLT2R or with the empty vector (pcDNA3.1(+)). Twenty-four hours after transfection, cells were incubated for 1.5 h at 37 °C with 20 μl/well Ca4 dye (FLIPR Calcium 4 Assay Kit, Molecular Devices) with 2.5 mM probenecid (an inhibitor of the anion-exchange protein). The dye was dissolved in HBSS-H (Hank's Balanced Salt Solution with 20 mM HEPES buffer, pH 7.4) supplemented with 0.4% BSA according to the manufacturer's instructions. Subsequently, the plate was equilibrated for 15 min before the start of measurement on a FlexStation II 384 Plate Reader (Molecular Devices) preheated to 37 °C. Ligands were diluted in HBSS-H supplemented with 0.4% BSA. Fluorescence was monitored over a 100-s time course, with readings taken every 2.5 s, and 10 μl/well of ligand was added to the FlexStation *in fluxo* 20 s after the start of measurement. The excitation and emission wavelengths were set, respectively, to 488 and 530 nm. Relative fluorescence units were calculated from the mean of each set of triplicate experiments for each time point and were used to generate a representative time course curve (Fig. 2b) derived with GraphPad Prism. The sigmoid dose response curve (Fig. 2c) was generated using the absolute peak magnitude signal, from which the signal for cells transfected with empty vector was subtracted to correct for background fluorescence. Data were normalized to the maximal calcium response elicited by wild-type CysLT2R with 100 nM LTD_4. Sigmoid dose response curves were calculated as the percentage of

$((RFU)_{CysLT2R} - (RFU)_{empty\ vector})$ versus ligand concentration with GraphPad Prism. EC_{50} values are means from seven independently repeated dose response curves.

Measurement of cAMP production ($G_{\alpha i}$ and $G_{\alpha s}$ biological assays)

cAMP production was monitored using the RLuc3-EPAC-GFP10 BRET2 biosensor as previously described [35]. The plasmid encoding the EPAC biosensor was a kind gift of M. Bouvier (Université de Montréal). Briefly, the EPAC protein, which changes its conformation upon cAMP binding, is tagged on each extremity of the protein with a BRET donor (*Renilla* luciferase, Rluc3) and a BRET acceptor (GFP10) to monitor intramolecular BRET signal. Activation of the $G_{\alpha s}$ and $G_{\alpha i}$ pathways is determined by measuring the BRET ratio, that is, the GFP10 (530 nm)/Rluc3 (480 nm) ratio, resulting from structural rearrangements within EPAC [35]. HEK293T cells were transiently cotransfected with empty vector (pcDNA3.1(+)) or vector encoding wild-type or Leu129Gln CysLT2R along with the RLuc3-EPAC-GFP10 cAMP sensor in 96-well plates. Twenty-four hours after transfection, cells were incubated with increasing concentrations of LTD_4 agonist with ($G_{\alpha i}$ coupling assay) or without ($G_{\alpha s}$ coupling assay) 4 μM forskolin (which maximally activates adenylyl cyclase and produces intracellular cAMP) at room temperature for 5 min before BRET readings. The luciferase substrate Coelenterazine DeepBlue C (5 μM final concentration; Biotum) was added 10 min before readings. BRET2 signal was monitored on a BioTek Synergy NEO plate reader. Cells transfected with vector encoding control receptor coupling to $G_{\alpha i}$ or $G_{\alpha s}$—CCR5 and CLR/RAMP2 receptors, respectively—and treated with increasing concentrations of RANTES or adrenomedullin agonist were used as controls in each experiment. Data are expressed as the percentage of cAMP accumulation relative to the maximal response obtained with forskolin induction and correspond to means ± s.e.m. from four ($G_{\alpha i}$ assay) and two ($G_{\alpha s}$ assay) independent experiments, in which each measurement was obtained in triplicate. Dose response curves were derived with GraphPad Prism.

Molecular modeling

Homology modeling of $CysLT_2R$ (UniProt, Q9NS75) was performed with the automodel routine of the software package MODELLER version 9.15 (ref. 36) using the crystal structure of human PAR1 (F2R/PAR1) [14] as a template (Protein Data Bank (PDB), 3VW7; UniProt, P25116). The sequence alignment provided as input for the automodel routine was generated with ClustalW [37] and manually refined in MacVector 14.0 (MacVector). Figures were generated using VMD 1.9.2 (ref. 38) to visualize residues 27–311 of the receptor, including the transmembrane helical bundle and the packing of the hydrophobic microdomain around Leu129 (3.43).

Flow cytometry

For FACS analysis of FLAG epitope on the cell surface, transiently transfected HEK293T cells were collected with PBS on ice, centrifuged at 350*g* and resuspended in FACS buffer (0.5 mM $MgCl_2$ and 0.1% BSA in PBS). Cells were then incubated with a monoclonal antibody to FLAG conjugated to Alexa Fluor 647 (R&D System, clone 1042E; 3 μl antibody/1 × 10^6 cells) on ice for 45 min. Cells were then washed in PBS, fixed in 2% formaldehyde, and analyzed on an LSR-Fortessa (BD Biosciences). To determine the percentage of NIH3T3 and melan-a cells with stable GFP expression, cells were collected,

centrifuged at 400*g* resuspended in FACS buffer (2% FBS, 5 mM EDTA, 25 mM HEPES, and 100 ng/ml DAPI), and analyzed on an LSR-Fortessa before subcutaneous injection into mice for xenograft experiments. Cells stably expressing GFP were sorted with a FACSAria II (BD Biosciences).

Cell lines and *in vitro* analysis

HEK293T cells were obtained from the American Type Culture Collection (ATCC) and were grown in DMEM (4.5 g/L glucose (Life Technologies)). Melan-a cells were provided by D. Bennett (St. George's Hospital, University of London) [15] and were grown in RPMI with 200 nM TPA (Sigma-Aldrich) unless noted otherwise. NIH3T3 mouse embryonic fibroblasts (CRL-1658) were obtained from ATCC and cultured in DMEM. MEL290 cells (a gift from T. Wiesner) were grown in RPMI. All cell culture media contained 10% FBS, penicillin (100 U/ml), streptomycin (100 μg/ml), and l-glutamine (2 mM). All cell lines tested negative for mycoplasma contamination. Cell growth was assessed using CellTiter-Glo (Promega), and the fold change in growth at day 3 was calculated relative to the day 1 luminescence values. Results from a representative experiment are shown; cell growth was assessed in three independent experiments, each with quadruplicate measures.

Immunoblotting

Cell lysates for melan-a cells were prepared in SDS lysis buffer (1% SDS, 20 mM NaF, and 5 mM EDTA) supplemented with fresh proteinase and phosphatase inhibitors (PhosSTOP, Roche; Complete EDTA-Free, Roche). HEK293T cells were collected in PBS containing 1% PMSF (Sigma-Aldrich) and 1% aprotinin (Sigma-Aldrich). Cell pellets were lysed in lysis buffer (PBS containing 50 mM Tris, pH 6.8, 100 mM NaCl, 1 mM $CaCl_2$, and 10% DM (dodecyl β-d-maltoside; Anatrace) supplemented with protease and phosphatase inhibitors (Complete EDTA-Free) for 1 h at 4 °C and subsequently centrifuged at 1000*g* for 15 min at 4 °C. Equal amounts of protein, as measured by BCA protein assay (Thermo Scientific) or Bradford protein assay (Bio-Rad), were resolved on NuPAGE Novex 4–12% Bis-Tris Protein Gels (Life Technologies) and transferred electrophoretically onto a 0.45-μm nitrocellulose membrane (Bio-Rad) or a PVDF membrane (Immobilon). Membranes were blocked for 1 h at room temperature in 5% milk in TBST or Odyssey blocking buffer (LI-COR) before being incubated overnight at 4 °C with primary antibodies diluted 1:1,000, unless otherwise noted, in either 5% milk in TBST or Odyssey blocking buffer. Antibodies to the following proteins were used: $CysLT_2R$ (Santa Cruz Biotechnology, E-20), MITF (Cell Signaling Technology, 12590), c-Kit (Cell Signaling Technology, 3074), gp100 (Abcam, ab137078), TRP2 (Abcam, ab74073), GFP (Abcam, ab6556), GAPDH (1: 5,000 dilution; Applied Biological Materials, G041), FLAG tag (1:3,000 dilution; Sigma-Aldrich, F7425), 1D4 tag (1:3,000 dilution; obtained from the National Cell Culture Center), and β-tubulin (1:500 dilution; Abcam, ab6046).

In vivo tumor formation

All mouse experiments were performed in accordance with a protocol approved by the MSKCC Institutional Animal Care and Use Committee (11-12-029). The size for each cohort was determined on the basis of previous experience without specific statistical methods. We resuspended 1×10^6 stably transduced melan-a or NIH3T3 cells in 100 μl of a

1:1 mix of medium and Matrigel (BD Biosciences) and subcutaneously and bilaterally injected the mix into the flanks of 7-week-old female CB17-SCID mice (Taconic). To assess tumor growth, five mice per group were injected for a total of ten tumors per group. No randomization or blinding was used in the analysis of tumor growth. A single tumor was excluded from the melan-a wild-type $CysLT_2R$ group because of deviation from the mean and erratic growth. Two tumors from the melan-a Leu129Gln $CysLT_2R$ group were excluded because of growth that differed from the mean. Melan-a *in vivo* tumor formation was assessed in two independent experiments, with the results of one experiment shown in Figure 2b. Tumors were measured with calipers every 2 or 3 d for up to 35 d. Growth curves were visualized with Prism GraphPad 6.0. Tumor volume was calculated using the formula

$$\text{volume} = \frac{\pi(\text{length})(\text{width})(\text{height})}{6}$$

For hematoxylin and eosin staining, tumors were fixed at 4 °C overnight in 4% paraformaldehyde. Tissue embedding in paraffin, sectioning, and staining with hematoxylin and eosin were performed by Histoserv. Tumor protein lysates were generated by homogenization of flash-frozen tissue in cell lysis buffer (1% Triton X-100, 50 mM HEPES, pH 7.4, 150 mM NaCl, 1.5 mM $MgCl_2$, 1 mM EGTA, 100 mM NaF, 10 mM sodium pyrophosphate, 1 mM sodium orthovanadate, and 10% glycerol, containing freshly added protease and phosphatase inhibitors (PhosSTOP and Complete EDTA-Free)).

RNA isolation and RT–qPCR

For cultured melan-a cells, RNA was isolated using the E.Z.N.A. Total RNA kit (Omega). For tumor tissue, RNA was isolated by homogenizing the tumors in Ribozol (Amresco) followed by RNA purification with the RNeasy Plus Mini kit (Qiagen).

For RT–qPCR, RNA was reverse transcribed using the High-Capacity cDNA Reverse Transcription kit (Applied Biosystems) and PCR was run using Power SYBR Green PCR Master Mix (Applied Biosystems) on a QuantStudio 6 Flex system (Applied Biosystems). Primer sequences are listed in **Supplementary Table 1**. Expression was normalized to that of the ribosomal protein *Rpl27*. Relative mRNA expression was plotted as $2^{-\Delta\Delta Ct}$ or $2^{-\Delta Ct}$. Each RT–qPCR was performed in at least triplicate and repeated in three different experiments.

siRNA

For siRNA experiments, the following pooled siRNAs were used: human *CYSLTR2* (SMARTpool ON-TARGETplus *CYSLTR2* siRNA, Dharmacon) and scrambled siRNA (ON-TARGETplus Non-Targeting Pool, Dharmacon). Transient transfection with siRNA was performed using Lipofectamine RNAiMAX reagent (Invitrogen), and siRNA was reverse transfected into cells according to the supplied protocol.

Immunofluorescence

Immunofluorescence images were acquired using an FSX100 Olympus inverted-base microscope with a 60× oil immersion objective. HEK293T cells were seeded at a density of 1×10^6 cells/well in six-well plates for 24 h before transfection. Twenty-four hours after transfection, cells were seeded and plated at a density of 300,000 cells/ml on coverslips in six-well plates. After 24 h, cells were fixed in cold methanol for 5 min, blocked in blocking buffer ($CaCl_2$/$MgCl_2$ (Life Technologies) and 0.5% BSA in PBS) for 30 min, and incubated with a mouse monoclonal antibody to 1D4 (1:2,000 dilution) and a rabbit polyclonal antibody to FLAG (1:1,000 dilution) for 1 h at room temperature. Cells were then washed ($CaCl_2$/$MgCl_2$ in PBS; 5 min, three times) and incubated with secondary antibody, either Alexa Fluor 488–conjugated anti-mouse antibody (1:500 dilution) (green) or Alexa Fluor 594–conjugated anti-rabbit antibody (1:500 dilution) (red) (Thermo Fisher, A-11029 and A-11012, respectively) for 30 min at room temperature. Non-specific secondary antibody signal was removed by washing with $CaCl_2$/$MgCl_2$ in PBS (5 min, three times), followed by a final incubation with Hoechst stain (1:15,000 dilution in $CaCl_2$/$MgCl_2$ in PBS) at room temperature for 5 min. Coverslips were mounted onto glass slides, which were stored at −20 °C before being visualized.

Statistics

All statistical comparisons between two groups in the qPCR and xenograft experiments were performed with GraphPad Prism 6.0 software and used a two-tailed parametric unpaired *t* test.

Acknowledgments

We gratefully acknowledge the members of the Molecular Diagnostics Service in the Department of Pathology and the Marie-Josée and Henry R. Kravis Center for Molecular Oncology. We thank T. Wiesner (MSKCC and Medical University of Graz) for the melan-a and MEL290 cell lines and intellectual input, D. Abramson for intellectual input, C. Kandoth and the TCGA for data sharing, M. Berger and N. Bouvier for obtaining patient DNA, Y.A. Berchiche for the flow cytometry analysis and scientific input, and M. Bouvier (Université de Montréal) for the kind gift of the EPAC construct. This work was supported in part by grants from the NIH to P.C. (P50CA140146, CDA; DP2CA174499; K08CA151660), the NIH to Y.C. (K08CA140946), the Sidney Kimmel Foundation to P.C. (Kimmel Scholar Award), the Cycle for Survival Fund to P.C. and Y.C., the Geoffrey Beene Award to P.C. and Y.C., the Prostate Cancer Foundation to Y.C., the STARR Cancer Consortium to P.C. and Y.C., and the François Wallace ç Monahan Fellowship to E.C.

References

1. Van Raamsdonk CD, et al. Frequent somatic mutations of *GNAQ* in uveal melanoma and blue naevi. Nature. 2009; 457:599–602. [PubMed: 19078957]
2. Van Raamsdonk CD, et al. Mutations in *GNA11* in uveal melanoma. N Engl J Med. 2010; 363:2191–2199. [PubMed: 21083380]
3. Johansson P, et al. Deep sequencing of uveal melanoma identifies a recurrent mutation in *PLCB4*. Oncotarget. 2016; 7:4624–4631. [PubMed: 26683228]
4. Furney SJ, et al. SF3B1 mutations are associated with alternative splicing in uveal melanoma. Cancer Discov. 2013; 3:1122–1129. [PubMed: 23861464]
5. Martin M, et al. Exome sequencing identifies recurrent somatic mutations in *EIF1AX* and *SF3B1* in uveal melanoma with disomy 3. Nat Genet. 2013; 45:933–936. [PubMed: 23793026]
6. Chang MT, et al. Identifying recurrent mutations in cancer reveals widespread lineage diversity and mutational specificity. Nat Biotechnol. 2016; 34:155–163. [PubMed: 26619011]

7. Leiserson MD, Wu HT, Vandin F, Raphael BJ. CoMEt: a statistical approach to identify combinations of mutually exclusive alterations in cancer. Genome Biol. 2015; 16:160. [PubMed: 26253137]
8. Harbour JW, et al. Frequent mutation of *BAP1* in metastasizing uveal melanomas. Science. 2010; 330:1410–1413. [PubMed: 21051595]
9. Harbour JW, et al. Recurrent mutations at codon 625 of the splicing factor *SF3B1* in uveal melanoma. Nat Genet. 2013; 45:133–135. [PubMed: 23313955]
10. Evans JF. Cysteinyl leukotriene receptors. Prostaglandins Other Lipid Mediat. 2002; 68–69:587–597.
11. Sakmar TP. Structure of rhodopsin and the superfamily of seven-helical receptors: the same and not the same. Curr Opin Cell Biol. 2002; 14:189–195. [PubMed: 11891118]
12. Ballesteros, JA.; Weinstein, H. Integrated methods for the construction of three-dimensional models and computational probing of structure-function relations in G protein–coupled receptors. In: Stuart, CS., editor. Methods in Neurosciences. Vol. 25. Academic Press; 1995. p. 366-428.
13. Tao YX. Constitutive activation of G protein–coupled receptors and diseases: insights into mechanisms of activation and therapeutics. Pharmacol Ther. 2008; 120:129–148. [PubMed: 18768149]
14. Zhang C, et al. High-resolution crystal structure of human protease-activated receptor 1. Nature. 2012; 492:387–392. [PubMed: 23222541]
15. Bennett DC, Cooper PJ, Hart IR. A line of non-tumorigenic mouse melanocytes, syngeneic with the B16 melanoma and requiring a tumour promoter for growth. Int J Cancer. 1987; 39:414–418. [PubMed: 3102392]
16. Prince S, Wiggins T, Hulley PA, Kidson SH. Stimulation of melanogenesis by tetradecanoylphorbol 13-acetate (TPA) in mouse melanocytes and neural crest cells. Pigment Cell Res. 2003; 16:26–34. [PubMed: 12519122]
17. Yaar M, Gilchrest BA. Human melanocyte growth and differentiation: a decade of new data. J Invest Dermatol. 1991; 97:611–617. [PubMed: 1940431]
18. Griewank KG, et al. Genetic and molecular characterization of uveal melanoma cell lines. Pigment Cell Melanoma Res. 2012; 25:182–187. [PubMed: 22236444]
19. Parma J, et al. Somatic mutations in the thyrotropin receptor gene cause hyperfunctioning thyroid adenomas. Nature. 1993; 365:649–651. [PubMed: 8413627]
20. Liu G, et al. Leydig-cell tumors caused by an activating mutation of the gene encoding the luteinizing hormone receptor. N Engl J Med. 1999; 341:1731–1736. [PubMed: 10580072]
21. Kan Z, et al. Diverse somatic mutation patterns and pathway alterations in human cancers. Nature. 2010; 466:869–873. [PubMed: 20668451]
22. Prickett TD, et al. Exon capture analysis of G protein–coupled receptors identifies activating mutations in *GRM3* in melanoma. Nat Genet. 2011; 43:1119–1126. [PubMed: 21946352]
23. Kandoth C, et al. Mutational landscape and significance across 12 major cancer types. Nature. 2013; 502:333–339. [PubMed: 24132290]
24. Lawrence MG, et al. A preclinical xenograft model of prostate cancer using human tumors. Nat Protoc. 2013; 8:836–848. [PubMed: 23558784]
25. Garraway LA, et al. Integrative genomic analyses identify *MITF* as a lineage survival oncogene amplified in malignant melanoma. Nature. 2005; 436:117–122. [PubMed: 16001072]
26. Leff JA, et al. Montelukast, a leukotriene-receptor antagonist, for the treatment of mild asthma and exercise-induced bronchoconstriction. N Engl J Med. 1998; 339:147–152. [PubMed: 9664090]
27. Wunder F, et al. Pharmacological characterization of the first potent and selective antagonist at the cysteinyl leukotriene 2 ($CysLT_2$) receptor. Br J Pharmacol. 2010; 160:399–409. [PubMed: 20423349]
28. Bond RA, Ijzerman AP. Recent developments in constitutive receptor activity and inverse agonism, and their potential for GPCR drug discovery. Trends Pharmacol Sci. 2006; 27:92–96. [PubMed: 16406086]
29. Langmead B, Salzberg SL. Fast gapped-read alignment with Bowtie 2. Nat Methods. 2012; 9:357–359. [PubMed: 22388286]

30. Li H, et al. The Sequence Alignment/Map format and SAMtools. Bioinformatics. 2009; 25:2078–2079. [PubMed: 19505943]
31. Robinson JT, et al. Integrative genomics viewer. Nat Biotechnol. 2011; 29:24–26. [PubMed: 21221095]
32. Cerami E, et al. The cBio cancer genomics portal: an open platform for exploring multidimensional cancer genomics data. Cancer Discov. 2012; 2:401–404. [PubMed: 22588877]
33. Cheng DT, et al. Memorial Sloan Kettering–Integrated Mutation Profiling of Actionable Cancer Targets (MSK-IMPACT): a hybridization capture-based next-generation sequencing clinical assay for solid tumor molecular oncology. J Mol Diagn. 2015; 17:251–264. [PubMed: 25801821]
34. Refaeli Y, Van Parijs L, Alexander SI, Abbas AK. Interferon γ is required for activation-induced death of T lymphocytes. J Exp Med. 2002; 196:999–1005. [PubMed: 12370261]
35. Leduc M, et al. Functional selectivity of natural and synthetic prostaglandin EP4 receptor ligands. J Pharmacol Exp Ther. 2009; 331:297–307. [PubMed: 19584306]
36. Martí-Renom MA, et al. Comparative protein structure modeling of genes and genomes. Annu Rev Biophys Biomol Struct. 2000; 29:291–325. [PubMed: 10940251]
37. Larkin MA, et al. Clustal W and Clustal X version 2.0. Bioinformatics. 2007; 23:2947–2948. [PubMed: 17846036]
38. Humphrey W, Dalke A, Schulten K. VMD: visual molecular dynamics. J Mol Graph. 1996; 14:33–38. 27–28. [PubMed: 8744570]

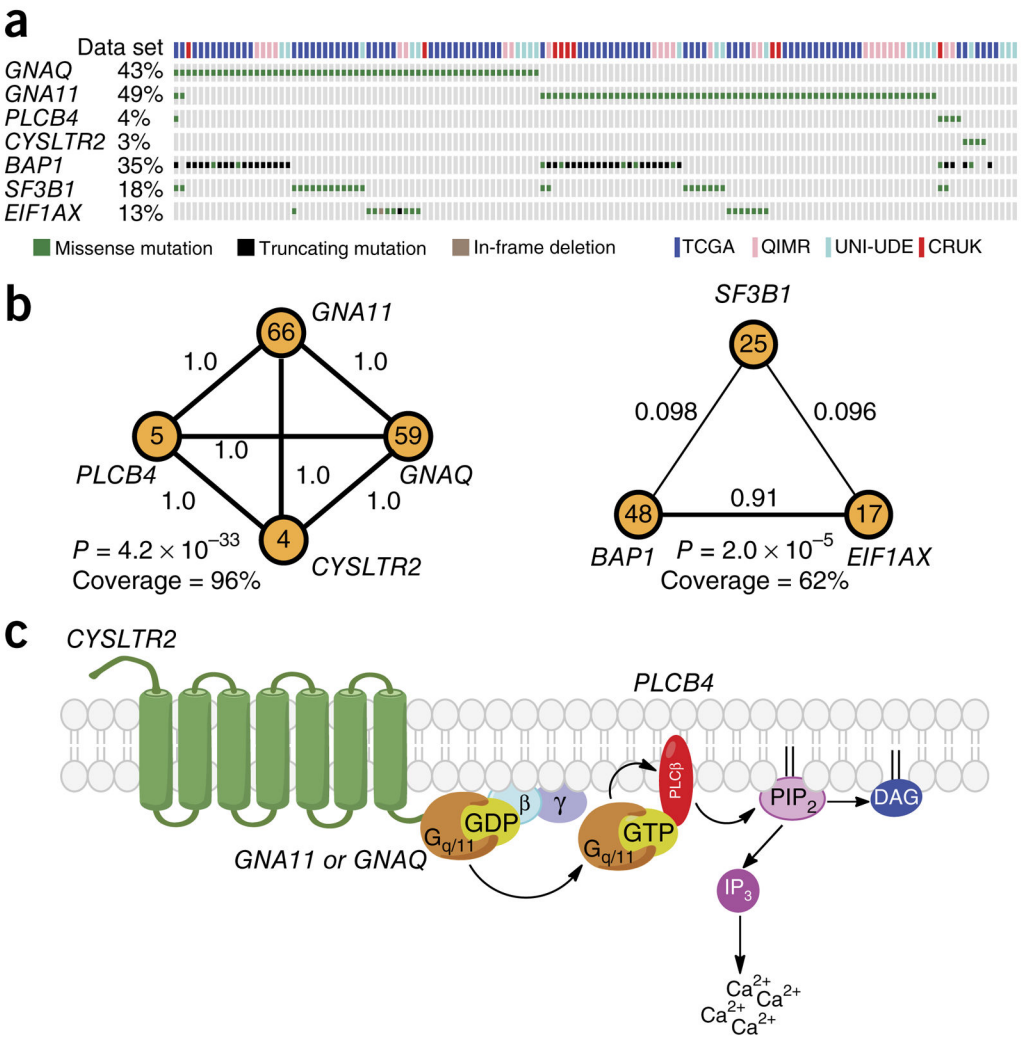

Figure 1.

CYSLTR2 mutation encoding p.Leu129Gln is a hotspot mutation and is mutually exclusive with known drivers in uveal melanoma. (**a**) OncoPrint of a selection of frequently mutated genes in uveal melanomas from four data sets: TCGA ($n = 80$), UNI-UDE ($n = 22$), CRUK ($n = 9$), and QIMR ($n = 25$). (**b**) CoMEt plots of two distinct, mutually exclusive modules in uveal melanoma. Each node is a mutated gene, and the number inside each node is the number of samples with a mutation in that gene. The number on each edge between nodes is edge weight (δ), which represents the fraction of permutations where mutations in the two genes are significantly mutually exclusive. The *P* value, also known as Φ, represents the mid *P* value that the genes in the module are mutated in a mutually exclusive manner. Coverage is the percentage of samples with at least one mutation in the genes in the module. (**c**) A schematic of the pathway activated in uveal melanoma. GPCR (*CYSLTR2*) activation of $G_{\alpha q/11}$ (*GNAQ* or *GNA11*) promotes the exchange of GDP for GTP and binding of $G_{\alpha q/11}$ to phospholipase C β (PLCβ; *PLCB4*) to activate cleavage of phosphatidylinositol 4,5-bisphosphate (PIP_2) to produce diacylglycerol (DAG) and inositol triphosphate (IP_3), resulting in subsequent calcium release.

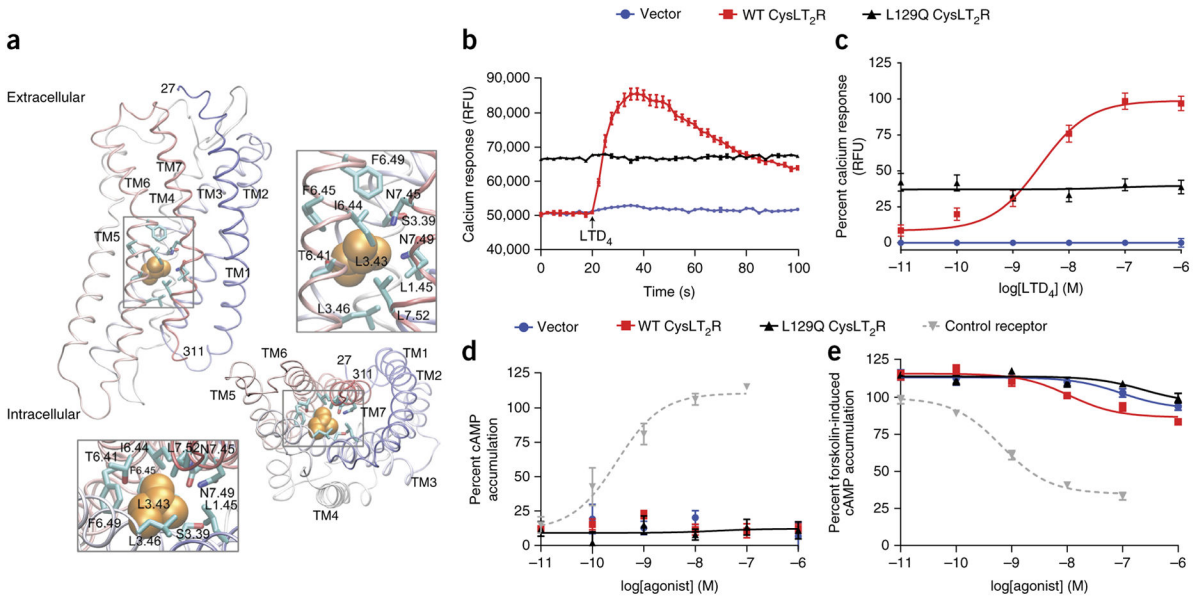

Figure 2.

Leu129Gln CysLT$_2$R exhibits high basal coupling to $G_{\alpha q}$. (**a**) Structural homology model of CysLT$_2$R based on the structure for PAR1. Transmembrane (TM) segments are labeled. Leu129 (3.43) is shown in orange space fill. Boxed segments are expanded to show residues that interact with position 3.43. The bottom panels show the model rotated by 90° relative to the top panels; the intracellular surface faces outward. (**b**) Representative 100-s time course of calcium flux with 10 nM LTD$_4$ added at 20 s (arrow) in HEK293T cells transfected with empty vector or expressing wild-type (WT) or Leu129Gln CysLT$_2$R. Data are presented as relative fluorescence units (RFU). Error bars, s.e.m. from three biological replicates, each with three technical replicates. (**c**) LTD$_4$ concentration-dependent calcium flux in HEK293T cells transfected with empty vector or expressing wild-type or Leu129Gln CysLT$_2$R. The EC$_{50}$ (half-maximal effective concentration) for wild-type CysLT$_2$R is 3.07 nM. Expression of Leu129Gln CysLT$_2$R causes sustained elevated calcium flux that is unaffected by LTD$_4$. Data are presented as the percentage of relative fluorescence units at LTD$_4$ concentrations and correspond to the means ± s.e.m. of seven independent experiments, each carried out in triplicate. (**d**) Dose-dependent $G_{\alpha s}$ activation by LTD$_4$ in HEK293T cells cotransfected with vector encoding RLuc3-EPAC-GFP10 together with empty vector or vector encoding wild-type or Leu129Gln CysLT$_2$R. An overlay shows activity for a control receptor (calcitonin receptor–like receptor (CLR); cotransfected with the RAMP2 accessory protein) in cells treated with adrenomedullin to cause dose-dependent production of cAMP. Data are expressed as the percentage of cAMP accumulation relative to that observed with forskolin induction and correspond to the means ± s.e.m. from two independent experiments, each carried out in triplicate. (**e**) Analysis of dose-dependent $G_{\alpha i}$ activation performed as in **d** with forskolin pretreatment. An overlay shows activity for a control receptor (C-C chemokine receptor 5 (CCR5)) in cells treated with RANTES to cause dose-dependent inhibition of forskolin-induced cAMP production. Data are expressed as the percentage of cAMP accumulation relative to that observed with forskolin induction and correspond to the means ± s.e.m. from four independent experiments, each carried out in triplicate.

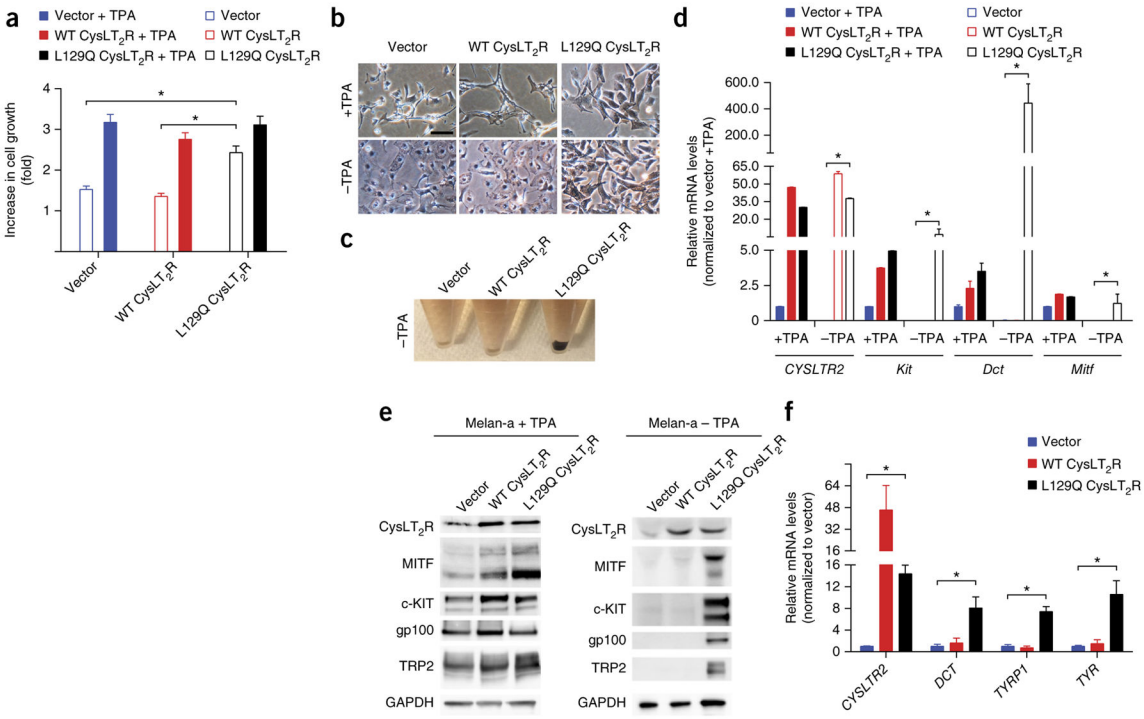

Figure 3.

Leu129Gln $CysLT_2R$ promotes TPA-independent growth *in vitro* and enforces a melanocyte-lineage-specific signature. (**a**) Cell growth of melan-a cells expressing empty-vector control, wild-type $CysLT_2R$, or Leu129Gln $CysLT_2R$ and assayed by CellTiter-Glo in the presence or absence of 200 nM TPA for 3 d. The fold increase in growth relative to cell numbers at 0 d is shown and corresponds to means ± s.e.m. from six technical replicates. **P* < 0.005. (**b**) Representative phase-contrast microscopy images of melan-a cells expressing empty-vector control, wild-type $CysLT_2R$, or Leu129Gln $CysLT_2R$ and grown in the presence or absence of 200 nM TPA for 3 d. Scale bar, 50 μm. (**c**) Cellular pellets of melan-a cells expressing empty-vector control, wild-type $CysLT_2R$, or Leu129Gln $CysLT_2R$ and grown in the absence of TPA for 18 d. (**d**) Relative mRNA levels of melanocyte-lineage-specific genes (*Kit*, *Dct*, and *Mitf*) in melan-a cells for each group in the presence or absence of 200 nM TPA for 18 d as assessed by RT–qPCR. Error bars, s.d. from three technical replicates. **P* < 0.05. (**e**) Cropped immunoblots of $CysLT_2R$ and melanocyte-lineage markers in melan-a cells expressing empty- vector control, wild-type $CysLT_2R$, or Leu129Gln $CysLT_2R$ and grown in the presence (left) or absence (right) of TPA for 18 d. Full-length immunoblots are presented in **Supplementary Figure 5**. (**f**) Relative mRNA expression of melanocyte-lineage-specific genes (*DCT*, *TYRP1*, and *TYR*) in MEL290 cells (a human melanoma cell line) expressing empty-vector control, wild-type $CysLT_2R$, or Leu129Gln $CysLT_2R$ and grown for 14 d as assessed by RT–qPCR. Error bars, s.d. from three technical replicates. **P* < 0.05.

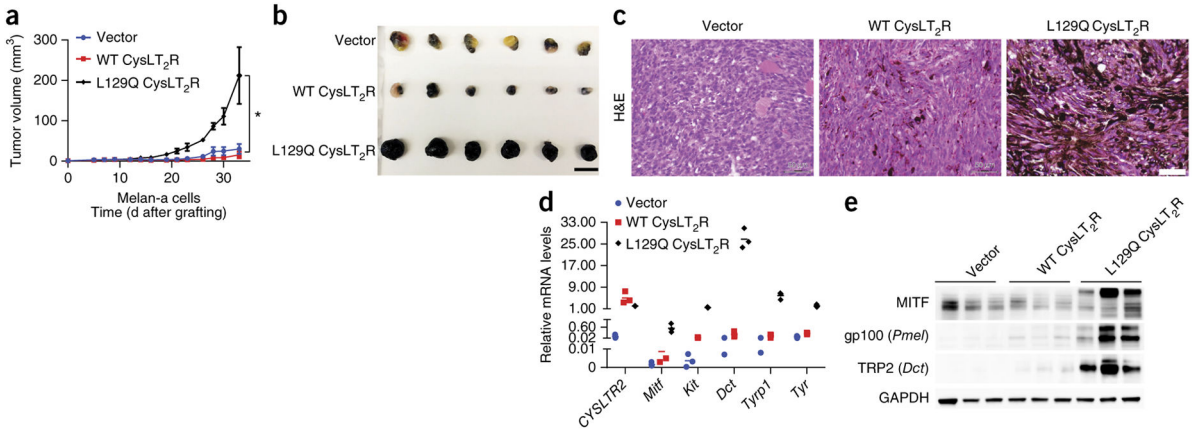

Figure 4.

Leu129Gln $CysLT_2R$ promotes tumorigenesis *in vivo* and enforces a melanocyte-lineage-specific signature. (**a**) Tumor volume over time of SCID mice subcutaneously injected with melan-a cells expressing empty-control vector, wild-type $CysLT_2R$, or Leu129Gln $CysLT_2R$ ($n = 8$ mice per group). Error bars, s.e.m.*$P < 0.001$. (**b**) Photograph of six representative melan-a xenograft tumors per group explanted at 32 d after implantation. Scale bar, 1.51 cm. (**c**) Representative hematoxylin and eosin (H&E) images of melan-a xenograft tumors expressing empty-vector control, wild-type $CysLT_2R$, or Leu129Gln $CysLT_2R$ at 32 d after implantation. Scale bar, 50 μm. (**d**) Relative mRNA levels of melanocyte-lineage-specific genes (*Mitf*, *Kit*, *Dct*, *Tyrp1*, and *Tyr*) assessed by RT–qPCR in three explanted xenograft tumors for each group. Each data point represents the mRNA level of a single tumor normalized to *Rpl27*. Statistical significance of $P < 0.05$ was observed for differences between tumors expressing Leu129Gln $CysLT_2R$ and tumors expressing empty-vector control or wild-type $CysLT_2R$. (**e**) Cropped immunoblots of $CysLT_2R$ and melanocyte markers in three explanted melan-a xenograft tumors for each group. Full-length immunoblots are presented in **Supplementary Figure 5**.

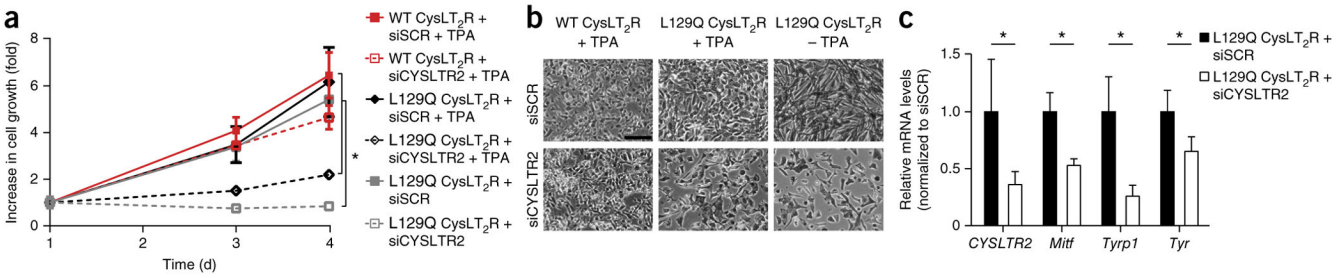

Figure 5.

CYSLTR2 is required for the growth and maintenance of the melanocyte-lineage-specific signature in melan-a cells transformed to express Leu129Gln $CysLT_2R$. (**a**) Growth curves of melan-a cells expressing wild-type or Leu129Gln $CysLT_2R$ transfected with either scrambled siRNA (siSCR) or siRNA targeting *CYSLTR2* (siCYSLTR2) and assayed by CellTiter-Glo. Melan-a cells expressing wild-type $CysLT_2R$ were grown in the presence of 200 nM TPA, whereas cells expressing Leu129Gln $CysLT_2R$ were grown in the presence or absence of 200 nM TPA. All cells were grown for 3 d. The fold increase in growth is shown relative to cell numbers at 1 d and corresponds to the means ± s.e.m. from six technical replicates. $*P < 0.05$. (**b**) Representative phase-contrast microscopy images of melan-a cells expressing wild-type or Leu129Gln $CysLT_2R$ transfected with either scrambled siRNA or siRNA targeting *CYSLTR2* at day 5 after transfection. Scale bar, 50 μm. (**c**) Relative mRNA levels of melanocyte-lineage-specific genes (*Mitf*, *Tyrp1*, and *Tyr*) in melan-a cells expressing Leu129Gln $CysLT_2R$ with scrambled siRNA or siRNA targeting *CYSLTR2* grown in the presence of TPA. Error bars, s.d. from three technical replicates. $*P < 0.05$.

Table 1

Recurrent hotspot mutations in uveal melanoma

Gene	Codon	Alteration[a]	Mutations at codon	Mutations in gene	*P* value	*q* value
GNA11	Gln209	p.Gln209Leu (64)	64	66	1.4×10^{-275}	3.3×10^{-272}
GNAQ	Gln209	p.Gln209Pro (40), p.Gln209Leu (15)	55	59	1.3×10^{-211}	3.0×10^{-208}
SF3B1	Arg625	p.Arg625His (10), p.Arg625Cys (8)	18	25	9.5×10^{-37}	9.6×10^{-33}
CYSLTR2	Leu129	p.Leu129Gln (4)	4	4	3.4×10^{-11}	7.5×10^{-8}
PLCB4	Asp630	p.Asp630Tyr (3), p.Asp630Phe (1), p.Asp630Asn (1)	5	5	3.0×10^{-10}	2.7×10^{-6}
SF3B1	Lys666	p.Lys666Thr (4)	3	35	3.0×10^{-7}	1.6×10^{-3}
EIF1AX	Gly6	p.Gly6Asp (2), p.Gly6Val (1)	3	16	3.0×10^{-6}	2.4×10^{-3}

[a]The number of tumors in which an alteration was present is given in parentheses.